On the distribution of ion density depletion along magnetic field lines as deduced using C/NOFS

E. Dao,[1] M. C. Kelley,[1] D. L. Hysell,[2] J. M. Retterer,[3] Y.-J. Su,[4] R. F. Pfaff,[5] P. A. Roddy,[4] and J. O. Ballenthin[4]

Received 6 December 2011; revised 8 March 2012; accepted 13 March 2012; published 1 May 2012.

[1] To investigate ion density depletion along magnetic field lines, we compare in situ-measured ion density fluctuations as seen from C/NOFS and compare them to the field-line-integrated depletion of the whole bubble as inferred from electric field measurements. Results show that, within C/NOFS' range, local measurement of the normalized density depletion, $\Delta n/n_0$, near the apex may be far less than at other points on the same field line. We argue that the distribution of $\Delta n/n_0$ is a weighted distribution concentrated at latitudes of the Appleton anomalies and becomes more heavily weighted the closer the field-aligned bubble rises to the peak of the anomalies. A three-dimensional simulation of an ionospheric bubble verifies our arguments.

Citation: Dao, E., M. C. Kelley, D. L. Hysell, J. M. Retterer, Y.-J. Su, R. F. Pfaff, P. A. Roddy, and J. O. Ballenthin (2012), On the distribution of ion density depletion along magnetic field lines as deduced using C/NOFS, *Radio Sci.*, *47*, RS3001, doi:10.1029/2011RS004967.

1. Introduction

[2] Since spread-F irregularities are field-aligned, the spread-F problem is often simplified by integrating three-dimensional (3D) physics along magnetic field lines into a two-dimensional problem, as first prescribed by *Perkins* [1973] for midlatitudes and by G. Haerendel (Theory of equatorial spread F, preprint, Max-Planck-Institut für Extraterrestrische Physik, Munich, Germany, 1973). However, to locate where scintillation will latitudinally occur, the distribution of irregularity along a field line is important. The problem is obfuscated by a lack of spread-F measurements along field lines. No radar is capable of the required latitudinal range. Satellite orbits cannot follow along field lines. Hence, we are limited to local measurements of spread F and to only a one-dimensional cut across a bubble. However, because of the high conductivity parallel to Earth's magnetic field, **B**, field lines are very accurately equipotential for scales greater than 1 km [*Kelley*, 2009], which is why spread F is field-aligned in the first place. From a single local electric field measurement, we are able to infer the electric field at any point along the field line, including those aligned with spread F. The electric field mapping along magnetic dipole field lines is derived in Appendix A. We later show that, from a single local electric field measurement, we can also infer the field-line-integrated ion density depletion. We analyze and interpret in situ measurements of ion density irregularities and compare them to inferred field-line-integrated depletions from electric field measurements as observed by the Communications/Navigation Outage Forecasting System (C/NOFS) satellite.

[3] Developed by the Air Force Research Laboratory, C/NOFS was launched to investigate the F region of the equatorial ionosphere. The vehicle orbits at an inclination of 13 degrees in reference to the geographic equatorial plane. The satellite orbit has a perigee of 400 km and an apogee of 850 km. Part of the satellite's payload is a Planar Langmuir Probe (PLP) [*Roddy et al.*, 2010], which measures ion density. C/NOFS also measures electric fields with the Vector Electric Field Instrument (VEFI) [*Pfaff et al.*, 2010]. With both PLP and VEFI, there is an abundance of simultaneous in situ ion density and electric field measurements. The data presented in this paper were measured from May 2008 through October 2009. Using PLP to measure the local ion density depletion at a local point and VEFI to infer the depletion along the whole field line, we explore the distribution of density depletion along field lines. To infer the depletion along an entire field line, we must first understand the dynamics of a bubble in three dimensions.

2. The Ion Density Perturbation Growth of Irregularities Along Field Lines

[4] Throughout this paper, we work in the frame of view moving with the $\mathbf{E} \times \mathbf{B}$ drift of the background electric field,

[1]School of Electrical and Computer Engineering, Cornell University, Ithaca, New York, USA.
[2]Department of Earth and Atmospheric Sciences, Cornell University, Ithaca, New York, USA.
[3]Institute for Scientific Research, Boston College, Chestnut Hill, Massachusetts, USA.
[4]Space Vehicles Directorate, Air Force Research Laboratory, Kirtland AFB, New Mexico, USA.
[5]Laboratory for Extraterrestrial Physics, NASA Goddard Space Flight Center, Greenbelt, Maryland, USA.

0048-6604/12/2011RS004967

$\mathbf{E}_0$. As derived in Appendix B, the current equation in this frame is

$$\mathbf{J} = \boldsymbol{\sigma} \cdot \Delta\mathbf{E} + \frac{nM\mathbf{g}' \times \mathbf{B}}{B^2} - \frac{\nabla p \times \mathbf{B}}{B^2}, \quad (1)$$

where $\mathbf{J}$ is the current density, $\boldsymbol{\sigma}$ is the conductivity tensor, $\mathbf{E}$ is the electric field, $\Delta\mathbf{E}$ is a perturbation electric field ($\Delta\mathbf{E} \equiv \mathbf{E} - \mathbf{E}_0$), n is ion density, M is ion mass, $\mathbf{B}$ is the magnetic field, and p is pressure. Note in this form that the background electric field is found in the effective gravity $\mathbf{g}' \equiv \mathbf{g} - \nu_{in}\mathbf{E}_0 \times \mathbf{B}/B^2$ where g is gravity, ν_{in} is the ion-neutral collision frequency, and $\mathbf{E}_0$ is the background electric field. Assuming that ∇p is vertical and that gravity is anti-vertical and they only drive zonal currents and zonal polarization electric fields, we restrict our focus to the zonal components of current equation (1):

$$J_x = \sigma_p \Delta E_x + \frac{nMg'}{B}\cos D - \frac{1}{B}\frac{\partial p}{\partial z}\cos D, \quad (2)$$

where σ_p is the Pedersen conductivity, ΔE_x is the zonal electric field perturbation, and D is the dip angle (the angle between the magnetic field and the horizon). Throughout the paper, we refer to x as being in the magnetic zonal direction, y as being parallel to the magnetic field, and z as being perpendicular to the magnetic field and in the meridional plane. The problem with (2) alone is that we must recognize that all of the points along a field line are approximately equipotential, as discussed earlier, and are thus effectively tied together. Every point along a field line has the same net zonal current as any other point on the line. Note that current observed at any specific point is not necessarily produced at that point locally. For instance, electric field-induced currents will flow through the paths of least resistance and not necessarily where the electric field is strongest. Regardless of how electric fields map along magnetic field lines, most of the current will flow through where the Pedersen conductivity is greatest. A more comprehensive current equation must be formulated.

[5] Take the circuit analogy of several current sources tied together in parallel. The output current of the parallel sources is the sum of all the sources. In our case, the current sources are driven by electric fields, gravity, and pressure gradients tied together in parallel by magnetic field lines. The total zonal current driven by any of the three drivers is a field-line integral of its current contribution. Dividing this integral by the length of the line yields the effective zonal current density. Using the electric field mapping for a dipole magnetic field (A1), the effective zonal current driven by electric fields is formulated as

$$J'_{xE} = \frac{\int \frac{\sigma_p}{\cos^3\theta} dy}{\int dy} \Delta E_x|_{\theta=0}, \quad (3)$$

where $\Delta E_x|_{\theta=0}$ is the electric field perturbation at the magnetic equator, θ is the magnetic latitude, and the integration in the y direction is along the magnetic field line. Turning to the other current contributions, we note that *Perkins* [1973] treats both gravity and pressure-gradient-driven currents as a varying value along the field line. However, similar to the formulation of Pedersen currents, both gravity-driven currents and pressure-driven currents are also tied together by magnetic field lines. The effective zonal currents should not differ from point to point along equipotential field lines. All points on a field line must be subjected to the same net zonal current, regardless of how much current is produced locally. Similar to the formulation of (3), we formulate the effective current density driven by gravity and pressure gradients in equations (4) and (5), respectively, as field-line integrals divided by the length of the field line:

$$J'_{x\ gravity} = \frac{\int \frac{nMg'}{B}\cos D dy}{\int dy}, \quad (4)$$

$$J'_{x\ pressure} = -\frac{\int \frac{1}{B}\frac{\partial p}{\partial z}\cos D dy}{\int dy}, \quad (5)$$

where D is the dip angle, the angle between the magnetic field and the horizon. Combining all of the effective current densities yields

$$J'_x = \frac{\int \frac{\sigma_p}{\cos^3\theta} dy}{\int dy} \Delta E_x|_{\theta=0} + \frac{\int \frac{nMg'}{B}\cos D dy}{\int dy} - \frac{\int \frac{1}{B}\frac{\partial p}{\partial z}\cos D dy}{\int dy}, \quad (6)$$

where the first, second, and third terms are the effective current densities driven by electric field, gravity, and pressure gradients, respectively. The new current equation (6) is similar to the equation of the locally produced current (2) except that all of the points along a field line are properly tied together and are actually common values to all points on equipotential field lines.

[6] To satisfy the quasi-neutrality of plasma, the current divergence must be zero ($\nabla \cdot J = 0$). Assume the plane wave solutions $\Delta E_x = \delta E_x e^{i(\omega t - kx)}$ and $\Delta n = \delta n\, e^{i(\omega t - kx)}$ where k is the zonal wave number and Δn is the ion density perturbation from the ambient density, n_0. The corresponding pressure is $p = p_0 + k_b\,(T_i + T_e)\Delta n$ where p_0 is the ambient pressure, k_B is the Boltzmann constant, T_i is the ion temperature, and T_e is the electron temperature. Taking the divergence of (6), setting it to zero, using the plane wave solutions, dropping second-order terms, and using the electric field mapping for dipole magnetic fields (A1), the linearization of the zonal current divergence equation yields

$$\delta E_x|_{\theta=0} = -\frac{\int \frac{Mg'\cos D}{B}\delta n\, dy}{\int \frac{\sigma_p}{\cos^3\theta} dy},$$
$$\Delta E_x = -\frac{1}{\sigma'_p}\frac{\int \frac{Mg'\cos D}{B}\Delta \mathrm{n}\, dy}{\int dy}, \quad (7)$$

where $\delta E_x|_{\theta=0}$ is δE_x, evaluated at the magnetic equator, and we define an effective Pedersen conductivity as $\sigma'_p \equiv$

$\cos^3(\theta) \cdot \int(dy \cdot \sigma_p/\cos^3\theta)/\int dy$. We neglect the second-order term involving the change in σ_p due to density perturbations for two reasons. For cases where Δn and ΔE_x are small compared to the ambient density and ambient zonal electric field, respectively, the second-order term is negligible. Second-order terms are often neglected in linear analyses. Even if Δn and ΔE_x are not small, the change in the effective Pedersen conductivity, σ_p', is negligible. Depletions are found in the F region and, while they affect σ_p in the F region, they will not significantly affect σ_p at lower altitudes. Since the effective Pedersen conductivity is dominated by σ_p in the minimally affected lower altitudes, neglecting the changes of σ_p due to density perturbations is justified. Equation (7) describes the polarization electric field that develops to relieve any current divergence due to density perturbations along a field line. Note that since $\partial(\Delta n)/\partial z$ is zero and the zonal divergence of $\partial p_0/\partial z$ is zero, pressure gradients have no zonal current divergence in our analysis and play no role in (7). A circuit analogy to ΔE_x as formulated by (7) is the voltage that results from several current sources and conductors in parallel with one another. The voltage across such a circuit would be the total current sources divided by the total conductance. In our case, the divergences of gravity-driven currents are current sources and the Pedersen conductivities are conductors, both of which are tied together in parallel by magnetic field lines.

[7] To formulate the ion density, perturbation growth of a bubble at a given point, we turn to the continuity equation in a frame of view moving with the gravitational and diamagnetic drift in addition to the frame moving with the $\mathbf{E} \times \mathbf{B}$ drift of the background electric field. Bubbles move with both gravitational and diamagnetic drifts and remain zonally fixed in this frame of view. The remaining velocity to consider is the $\mathbf{E} \times \mathbf{B}$ drift of ΔE_x. Assuming the plasma is incompressible ($\nabla \cdot \mathbf{v} = 0$) and neglecting recombination, which we assume is much slower than the processes of spread F, the continuity equation becomes

$$\begin{aligned} \frac{\partial n}{\partial t} + \nabla \cdot (n\mathbf{v}) &= 0, \\ \frac{\partial n}{\partial t} &= -\frac{\partial n_0}{\partial z}\frac{\Delta E_x}{B}, \end{aligned} \tag{8}$$

which describes the growth rate of the density perturbation at any point in a bubble. From (7), ΔE_x is the opposite sign of Δn. Hence, density perturbations grow where $\partial n_0/\partial z$ is positive. In other words, density perturbations grow below the F peak. For a sense of the variation of the density perturbation growth rate (8) along a field line, we model the varying B and ΔE_x along a field line. Modeling B as a magnetic dipole such that $B = \left(\sqrt{1+3\sin^2\theta}/\cos^6\theta\right) \cdot B|_{\theta=0}$ where $B|_{\theta=0}$ is the magnetic field at the equator and using the zonal electric field-mapping equation (A1), we can recast (8) as

$$\begin{aligned} \frac{\partial n}{\partial t} &= -\frac{\cos^3\theta}{\sqrt{1+3\sin^2\theta}}\frac{\partial n_0}{\partial z}\frac{\Delta E_x\big|_{\theta=0}}{B\big|_{\theta=0}}, \\ \Delta n &= -\frac{\cos^3\theta}{\sqrt{1+3\sin^2\theta}}\int \frac{\partial n_0}{\partial z}\frac{\Delta E_x\big|_{\theta=0}}{B\big|_{\theta=0}}dt. \end{aligned} \tag{9}$$

[8] Note that $\Delta E_x|_{\theta=0}$ and $B|_{\theta=0}$ are global values shared by all points on the same field line whereas θ and $\partial n_0/\partial z$ are local values. How much the density perturbation at a point along a field line grows relative to other points on the field line is determined by its magnetic latitude and the local gradient of the background ion density. It is apparent from the $\cos^3\theta/\sqrt{1+3\sin^2\theta}$ factor that the greater the distance from the equator, the greater the local density perturbation growth attenuation. The attenuation of irregularities away from the equator can be seen in the work by *Dao et al.* [2011, Figure 2] where plasma irregularities are shown to straddle the magnetic equator, as observed by C/NOFS.

3. Inferring Field-Line-Integrated Ion Density Depletion From Electric Fields

[9] From equations (7)–(9) describing the dynamics of bubble growth, we can infer the field-line-integrated depletion from a single measurement of ΔE_x at any point on the field line. In equation (7) describing the polarization electric field induced by a bubble, we believe the integral in the numerator is dominated at the F peak. As suggested by the growth rates in equations (8) and (9), Δn maximizes near the F peak. Also, considering that most of the gravity-driven currents exist at the F peak where the ion density is greatest, most of the current divergence must happen near the F peak. We thus approximate equation (7) as

$$\Delta E_x \cong -\frac{1}{\sigma_p'}\left\langle \frac{Mg'\cos D}{B}\right\rangle \frac{\int \Delta n\, dy}{\int dy}, \tag{10}$$

where we define

$$\left\langle \frac{Mg'\cos D}{B}\right\rangle \equiv \frac{\int n_o^\alpha \frac{Mg'\cos D}{B} dy}{\int n_o^\alpha dy} \tag{11}$$

as a weighted average, concentrated where we assume the majority of Δn is located: near the F peak. The variable α is a tunable parameter controlling how much weight to emphasize at the F peak. Modeling B and the field lines with the International Geomagnetic Reference Field (IGRF), M from the International Reference Ionosphere (IRI) model [*Bilitza and Reinisch*, 2008], and σ_p and ν_{in} from both the IRI and the mass spectrometer incoherent scatter model (MSIS), we can infer the total depletion of a bubble along a field line from VEFI after re-arranging equation (10) as

$$\Delta N \equiv \int \Delta n\, dy \cong -\frac{\sigma_p' \int dy}{\left\langle \frac{Mg'\cos D}{B}\right\rangle} \cdot \Delta E_x. \tag{12}$$

[10] The field-line conductivity is still greater than the Pedersen conductivity into E region altitudes, even at night. Hence, when inferring ΔN, we integrate as low as 90 km. We do not consider anything below 90 km altitude because the increased ion-neutral collisions reduce the Pedersen

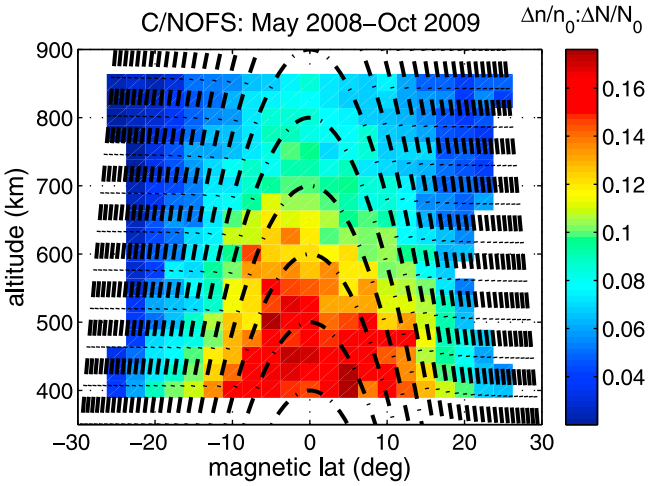

Figure 1. Average $\Delta n/n_0$:$\Delta N/N_0$ from May 2008 to October 2009 where $\Delta N/N_0$ is inferred from ΔE_x. The dotted-dashed lines represent dipole magnetic field lines. The higher the apex height of each field line, the smaller $\Delta n/n_0$:$\Delta N/N_0$ is, indicating a much greater $\Delta n/n_0$ somewhere farther down the intersecting field line.

conductivity significantly and we expect minimal zonal current below this altitude. Note that because we do integrate to such low altitudes, one cannot approximate the ion gyro frequency to be much greater than the ion-neutral collision when computing the local Pedersen conductivity, which is $\sigma_p = e^2\nu_{in}n/M(\nu_{in}^2 + \Omega_i^2)$ where Ω_i is the ion gyro frequency.

4. Data Representation: C/NOFS Ion Density and Electric Field Measurements

[11] From the C/NOFS' PLP, we derive the ambient density, n_0, as 60-s (~450 km spatially) averages of measured density. Subtracting n_0 from the density measurements yields the density deviation, Δn. We normalize the deviation by the background density as $\Delta n/n_0$. We determine ΔE_x from VEFI similarly as Δn, deriving the ambient zonal electric field as 60-s averages of the zonal electric field measurements and then subtracting it from the same measurements. Using equation (12), we then infer ΔN from ΔE_x. We also compute $N_0 \equiv \int n_0 dy$ from IRI and normalize the field-line-integrated depletion as $\Delta N/N_0$. We use the normalized parameter $\Delta N/N_0$ as opposed to the absolute ΔN because if the density profiles from IRI are off by a factor when computing the numerator, this factor is roughly canceled out by the denominator. We now focus our attention on the ratio $\Delta n/n_0$:$\Delta N/N_0$, which relates the local $\Delta n/n_0$ to that of the whole field line. The ratio indicates to what extent the local $\Delta n/n_0$ exceeds that of the whole field line ($\Delta n/n_0$:$\Delta N/N_0 > 1$) or is below that of the whole bubble ($\Delta n/n_0$:$\Delta N/N_0 < 1$). Note that $\Delta n/n_0$:$\Delta N/N_0$ is highly sensitive to noise as $\Delta N/N_0$ approaches zero. To remedy this issue in our statistical study, we compute the 60-s mean of the magnitude of $\Delta n/n_0$ and $\Delta N/N_0$ separately and present $\Delta n/n_0$:$\Delta N/N_0$ as the ratio between these two mean magnitudes. We restrict our focus to irregularities, so in our data presentation, we only use data where either of the mean magnitudes of $\Delta n/n_0$ or $\Delta N/N_0$ exceeded 10%. The average $\Delta n/n_0$:$\Delta N/N_0$ is binned by magnetic latitude and altitude, as shown in Figure 1. The dotted-dashed lines trace dipole magnetic field lines. The ratio $\Delta n/n_0$:$\Delta N/N_0$ is nearly symmetric across the magnetic equator. We attribute the slight asymmetry to the asymmetry of Earth's magnetic field.

5. Discussion

[12] As evident from equations (7) and (9), determining the distribution of ion density along the field line can be complex, beginning from an initial perturbation and then depending on the time evolution of (7) and (9). The complexity results from the local growth rate of Δn being dependent on the collective Δn along the whole field line, as dictated by (7), while the growth rate of Δn all along the field line also depends on unique local conditions. Further complicating the problem, the rise velocity of the bubble varies as a function of altitude, bubble size, and the time-varying background electric field [*McDaniel and Hysell*, 1997]. These considerations aside, we consider another important factor in the distribution of ion density irregularity along a field line: the latitudinal variation of plasma density profiles. To illustrate, we make a zero-order approximation that the ratio of $\Delta E_x|_{\theta=0}/B_x|_{\theta=0}$ to the rise velocity ($V \equiv dz/dt$) is constant, the $\cos^3\theta/(1 + 3\sin^2\theta)$ factor is approximately unity, and the gradient of n_0 is roughly in the z direction. Equation (9) can then be approximated as

$$\Delta n \sim -\frac{\Delta E_x|_{\theta=0}}{B_x|_{\theta=0}}\frac{1}{V}n_0. \tag{13}$$

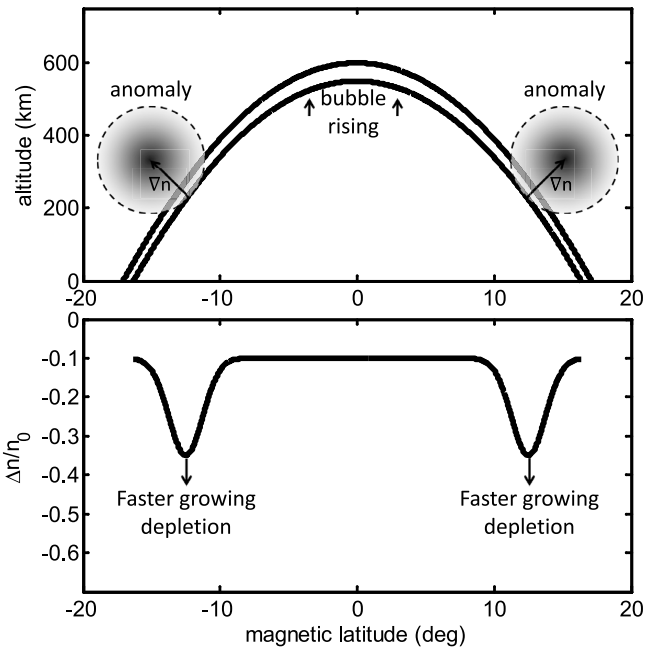

Figure 2. Schematic of a bubble rising through the Appleton anomalies where gray shading indicates the ion density of the anomalies. The bubble locally grows most rapidly where the gradients in the z direction are the greatest, beneath the anomalies' peaks. The resulting $\Delta n/n_0$ distribution concentrates near the anomalies.

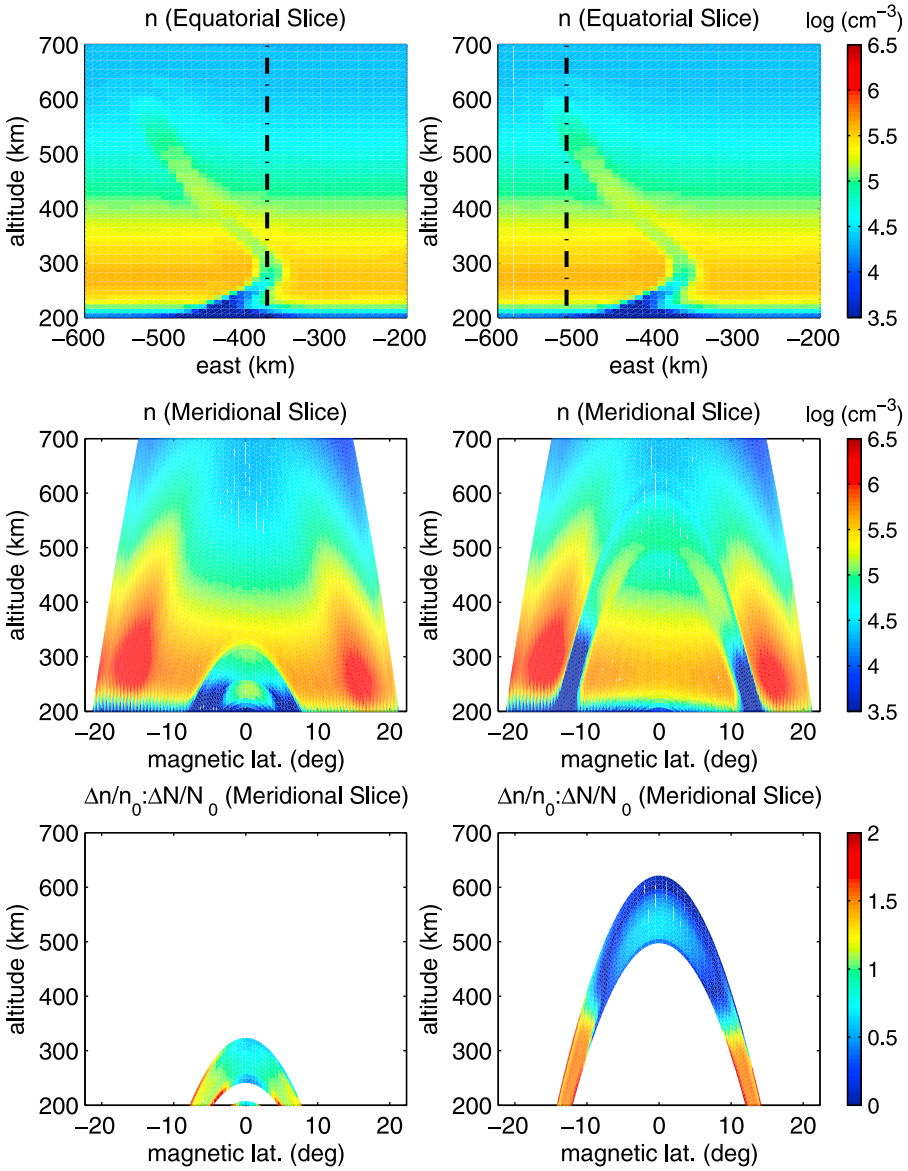

Figure 3. Snapshot of 3D bubble simulation. (top) An equatorial slice of the bubble's ion density in units of log(cm^{-3}). The dotted-dashed lines indicate the meridional slices that are examined in their respective columns. (middle) The ion density of the mentioned meridional slices. (bottom) The computed $\Delta n/n_0$:$\Delta N/N_0$ of the bubble. The part of the bubble rising closer to the Appleton anomalies yields a heavier distribution of $\Delta n/n_0$ near the anomalies.

[13] Equation (13) suggests that Δn is roughly proportional to n_0. If the density profile was latitudinally independent along the magnetic field line, the distribution of normalized density depletion, $\Delta n/n_0$, will be approximately uniform after dividing each side of (13) by n_0. This would be a tremendous coincidence, allowing us to infer Δn at any point along the same field line from a single measurement of $\Delta n/n_0$ by simply inferring n_0 at the point of interest with an ion density model. However, density profiles do vary with latitude, especially in the presence of the Appleton anomalies. Consider the schematic of a bubble rising through the anomalies shown in Figure 2 where the gray shading represents the ion density of the anomalies. Before approaching anomalies where the density profiles vary less significantly with latitude, we can expect a more uniform distribution of $\Delta n/n_0$ throughout the bubble. However, as a bubble rises, the local points approaching the anomalies experience greater density z-gradients than other points along the bubble. Consequently, the density perturbation grows rapidly at the points near the anomalies and the resulting $\Delta n/n_0$ distribution becomes heavily weighted there as well. Because most of the depletion occurs near the anomalies, $\Delta n/n_0$:$\Delta N/N_0$ increases near the anomalies while decreasing at other points such as the apex (where the C/NOFS observations presented in Figure 1 were observed).

[14] During 2008 and 2009, when the data presented were collected, the solar flux was at a minimum at around 60 solar flux units. Under such conditions, the F peak and the

Appleton anomalies were about 300–350 km high (below C/NOFS) and the apex altitude (the height of the apex of the intersecting field line) of the Appleton anomalies was about 800–900 km high (the upper limit of C/NOFS' range). Within C/NOFS' range (400–850 km), the observed irregularities with higher apex altitudes were ones that have risen closer to the Appleton anomalies. We expect the irregularities with higher apex altitudes to have a $\Delta n/n_0$ distribution increasingly concentrated near the anomalies, resulting in decreasing $\Delta n/n_0$:$\Delta N/N_0$ at CNOFS' point of observation. As seen in Figure 1, $\Delta n/n_0$:$\Delta N/N_0$ actually decreases with increasing apex altitudes. From a more careful inspection of $\Delta n/n_0$:$\Delta N/N_0$ along any given field line, $\Delta n/n_0$:$\Delta N/N_0$ increases farther away from the equator. We attribute this phenomenon to increasing density z-gradients away from the equator, approaching the latitudes of the anomalies. Unfortunately, C/NOFS' range does not extend to the anomalies at any time where we expect $\Delta n/n_0$:$\Delta N/N_0 > 1$. We turn to numerical 3D modeling to check the consistency of our arguments.

[15] We present the use of a 3D ionospheric model outlined by *Retterer* [2005, 2010] to calculate both global ambient ionospheric structure and 3D bubble simulation. The ambient model solves the continuity equation for plasma density in terms of the processes of production, loss, and transport of plasma density along and perpendicular to geomagnetic flux tubes in the vicinity of the geomagnetic equator. It requires specification of the solar UV flux, neutral densities, winds, and temperatures within the thermosphere, along with plasma drift velocity and temperature. For this study, empirical models of these parameters were used: the Mass Spectrometer and Incoherent Scatter (MSIS) model [*Hedin*, 1987] for neutral densities and temperatures, the Horizontal Wind Model (HWM) [*Hedin et al.*, 1991] for neutral winds, the *Hinteregger et al.* [1981] model for the solar ultraviolet spectrum, the *Scherliess and Fejer* [1999] model for plasma drifts, and the *Gulyaeva and Titheridge* [2006] model for the plasma temperature. We specify the F10.7 to be 60 solar flux units in the simulation presented in this paper. After the ambient conditions are computed, a 3D bubble simulation is done as described by *Retterer* [2010].

[16] A sinusoidal perturbation with a wavelength of 1200 km was initiated and we took a snapshot of the bubble as it rose to an altitude of 600 km, as shown in Figure 3. Figure 3 (top) is an equatorial slice of the bubble's ion density in units of log(cm^{-3}). The dotted-dashed lines indicate the meridional slices that are examined in their respective columns. Figure 3 (middle) presents the ion density of the mentioned meridional slices. We compute $\Delta n/n_0$:$\Delta N/N_0$ of the bubble in Figure 3 (bottom). In Figure 3 (left), a meridional cut of the bubble far below the anomalies, the $\Delta n/n_0$ distribution is nearly uniform with a $\Delta n/n_0$:$\Delta N/N_0$ near unity, indicating that Δn is roughly proportional to n_0. However, in Figure 3 (right), we show a slice of the bubble rising closer to the anomalies. As expected, the weight of the $\Delta n/n_0$ distribution lies heavier where the bubble intersects with the Appleton anomalies. Consequentially, $\Delta n/n_0$:$\Delta N/N_0$ is significantly greater than one at the Appleton anomalies and significantly less than one about the equator where the bubble does not pass though the anomalies. This is consistent with C/NOFS data representation and supports our argument of a heavy distribution of $\Delta n/n_0$ near the Appleton anomalies as bubbles approach them.

6. Conclusion

[17] The distribution of an ion density bubble along a field can be quite complicated since it depends on the time history of the bubble rise, starting from the initial perturbation and continuing with varying local conditions that impose varying local growth rates of Δn along the bubble. In the presence of Appleton anomalies, $\Delta n/n_0$ cannot be approximated as being constant along field lines. The data presented in this paper suggest that any local measurement of $\Delta n/n_0$ near the apex of a field line is only a very small fraction of the total field-line-integrated $\Delta N/N_0$, more so when the bubble intersects the Appleton anomalies. We note that a lot of variation existed in the data. This comes as no surprise, since longitudinal variability (realistic magnetic field, Appleton anomalies, tidal effects, etc.) as well as day-to-day variability, such as varying levels of solar flux, occurred during the span of 2008 to 2009.

[18] An implication of this study is that local measurements of $\Delta n/n_0$ or Δn at the equator cannot be trivially extended to higher latitudes in an effort to calculate scintillations at these latitudes. However, with equation (12), we show a means to estimate the density depletion of whole field lines from local zonal electric field perturbations, ΔE_x. Equation (13) suggests that the distribution of Δn is similar to the distribution of n_0 along the field line, so one may infer $\Delta n/n_0$ or Δn at any point along a field line from a single measurement of ΔE_x in conjunction with an ion density model. This calls for further investigation. We plan to test this approach using scintillation data from the -74° longitude chain [*Valladares et al.*, 2004]. Since C/NOFS' launch, up until now, scintillations have been low at GPS frequencies, but as solar activity increases, this comparison may be possible.

[19] Also, for increased solar activity, we hope to perform the same calculations as presented in this paper. The most significant change would be a higher F peak associated with higher solar flux. Under these conditions, C/NOFS may intersect the Appleton anomalies where we expect $\Delta n/n_0$:$\Delta N/N_0$ to exceed unity.

Appendix A: Electric Field Mapping for Magnetic Dipole

[20] While magnetic field lines are equipotential, the distance between field lines does vary. Approximating the Earth's magnetic field as a dipole magnetic field, $r = R_0 \cos^2\theta$ where r is the distance from the center of the Earth, R_0 is the r of the field line at the magnetic equator, and θ is the magnetic latitude. The zonal (x direction) electric field along a field line can be formulated as

$$\begin{aligned} E_x &= -\frac{d\Phi}{dx} = -\frac{d\Phi}{r\cos\theta d\lambda,} \\ E_x &= -\frac{d\Phi}{R_0\cos^3\theta d\lambda,} \\ E_x &= \frac{1}{\cos^3\theta}\cdot E_x|_{\theta=0}, \end{aligned} \tag{A1}$$

where Φ is the potential, λ is magnetic longitude, and $E_x|_{\theta=0}$ is the zonal electric field at the equator. Using the magnetic dipole identity, $\sin D = dz/(r{\cdot}d\theta)$, the derivative of R_0 with respect to magnetic latitude $dR_0/d\theta = 2r\sin\theta/\cos^3\theta$, and the dipole relationship $\sin D = 2\sin\theta/\sqrt{1+3\sin^2\theta}$ where D is the angle between the Earth's magnetic field and the horizon, the meridional (z direction) electric field along a field line is formulated as

$$\begin{aligned} E_z &= \frac{d\Phi}{dz} = \frac{d\Phi}{rd\theta\sin D}, \\ E_z &= d\Phi\frac{1}{r}\frac{2r\sin\theta}{dR_0\cos^3\theta}\frac{\sqrt{1+3\sin^2\theta}}{2\sin\theta}, \\ E_z &= \frac{d\Phi}{dR_0}\frac{\sqrt{1+3\sin^2\theta}}{\cos^3\theta}, \\ E_z &= \frac{\sqrt{1+3\sin^2\theta}}{\cos^3\theta}\,.\,E_z|_{\theta=0}, \end{aligned} \tag{A2}$$

where $E_z|_{\theta=0}$ is the meridional electric field at the equator. Both (A1) and (A2) are equivalent to expressions given by *Mozer* [1970], generalized for an arbitrary point on a field line instead of strictly where the field lines intersect the Earth's surface.

Appendix B: Current Density in a Frame Moving with E × B Drift of the Background Electric Field

[21] The momentum equation in the neutrals frame of view is well known and can be written as

$$nm\frac{d}{dt}\mathbf{v} = nq(\mathbf{E}+\mathbf{v}\times\mathbf{B}) + nm\mathbf{g} - \nabla p - nm\nu_n\mathbf{v}, \tag{B1}$$

where n is the ion or electron density, m is mass, $\mathbf{v}$ is ion velocity, q is charge, $\mathbf{E}$ is the electric field, $\mathbf{B}$ is the magnetic field, $\mathbf{g}$ is gravity, ∇p is the pressure gradient, and ν_n is the collision frequency with neutrals. In the frame moving with the $\mathbf{E}\times\mathbf{B}$ drift of the background electric field, $\mathbf{E}_0$, we make the transformation, $\mathbf{v} \rightarrow \mathbf{v} + \mathbf{E}_0\times\mathbf{B}/B^2$. Equation (B1) becomes

$$\begin{aligned} nm\frac{d\mathbf{v}}{dt} &= nq(\Delta\mathbf{E}+\mathbf{v}\times\mathbf{B}) + nm\mathbf{g} - \nabla p - nm\nu_n\left(\mathbf{v}+\frac{\mathbf{E}_0\times\mathbf{B}}{B^2}\right), \\ nm\frac{d\mathbf{v}}{dt} &= nq(\Delta\mathbf{E}+\mathbf{v}\times\mathbf{B}) + nm\mathbf{g}' - \nabla p - nm\nu_n\mathbf{v}, \end{aligned} \tag{B2}$$

where we define the effective gravity, $\mathbf{g}' \equiv \mathbf{g}' + \nu_n\,\mathbf{E}_0\times\mathbf{B}/B^2$, as was done by *Ott* [1978]. Solving for $\mathbf{v}$ in steady state ($d\mathbf{v}/dt = 0$) yields

$$\mathbf{v} = \begin{pmatrix} \frac{1}{\kappa^2+1} & 0 & \frac{\kappa}{\kappa^2+1} \\ 0 & 1 & 0 \\ -\frac{\kappa}{\kappa^2+1} & 0 & \frac{1}{\kappa^2+1} \end{pmatrix}.\left(\frac{q}{m\nu_n}\Delta\mathbf{E} + \frac{\mathbf{g}'}{\nu_n} - \frac{\nabla p}{nm\nu_n}\right), \tag{B3}$$

where κ is the gyro-to-collision frequency ratio ($\kappa \equiv qB/m\nu_n$) and we take y to be in the direction of the magnetic field. We take x and z to be perpendicular to the magnetic field in the zonal and meridional directions, respectively. Subtracting the ion velocity from the electron velocity and multiplying the difference by the ion/electron density and electron charge, e, yields the current density equation in the frame of view moving with the $\mathbf{E}\times\mathbf{B}$ drift of the background electric field:

$$\mathbf{J} = \boldsymbol{\sigma}\cdot\Delta\mathbf{E} + \frac{nM\mathbf{g}'\times\mathbf{B}}{B^2} - \frac{\nabla p\times\mathbf{B}}{B^2}, \tag{B4}$$

where M is the ion mass and we assumed that $\kappa \gg 1$. The conductivity tensor, $\boldsymbol{\sigma}$, is

$$\boldsymbol{\sigma} = \begin{pmatrix} \sigma_p & 0 & \sigma_h \\ 0 & \sigma_0 & 0 \\ -\sigma_h & 0 & \sigma_p \end{pmatrix}, \tag{B5}$$

where σ_p, σ_h, σ_0, are the Pedersen, Hall, and parallel conductivities, respectively.

[22] **Acknowledgments.** The C/NOFS mission is supported by the Air Force Research Laboratory, the Department of Defense Space Test Program, the National Aeronautics and Space Administration, the Naval Research Laboratory, and the Aerospace Corporation. The analysis was supported in part by NASA grants NNH09AK05I and NNH09AM20I to the Air Force Research Laboratory. Work at Cornell was funded by the Office of Naval Research under grant N00014-09-1-0975.

References

Bilitza, D., and B. W. Reinisch (2008), International Reference Ionosphere 2007: Improvements and new parameters, *Adv. Space Res.*, *42*, 599–609, doi:10.1016/j.asr.2007.07.048.

Dao, E., M. C. Kelley, P. Roddy, J. Retterer, J. O. Ballenthin, O. de la Beaujardiere, and Y.-J. Su (2011), Longitudinal and seasonal dependence of nighttime equatorial plasma density irregularities during solar minimum detected on the C/NOFS satellite, *Geophys. Res. Lett.*, *38*, L10104, doi:10.1029/2011GL047046.

Gulyaeva, T. L., and J. E. Titheridge (2006), Advanced specification of electron density and temperature in the IRI ionosphere-plasmasphere model, *Adv. Space Res.*, *38*, 2587–2595, doi:10.1016/j.asr.2005.08.045.

Hedin, A. E. (1987), MSIS-86 thermospheric model, *J. Geophys. Res.*, *92*, 4649–4662, doi:10.1029/JA092iA05p04649.

Hedin, A. E., et al. (1991), Revised global model of thermosphere winds using satellite and ground-based observations, *J. Geophys. Res.*, *96*, 7657–7688, doi:10.1029/91JA00251.

Hinteregger, H. E., K. Fukui, and B. R. Gilson (1981), Observational, reference and model data on solar EUV, from measurements on AE-E, *Geophys. Res. Lett.*, *8*(11), 1147–1150, doi:10.1029/GL008i011p01147.

Kelley, M. C. (2009), *The Earth's Ionosphere: Plasma Physics and Electrodynamics*, 2nd ed., Academic, Burlington, Mass.

McDaniel, R., and D. Hysell (1997), Models and DE II observations of inertial-regime irregularities in equatorial spread *F*, *J. Geophys. Res.*, *102*(A10), 22,233–22,246, doi:10.1029/97JA02038.

Mozer, F. S. (1970), Electric field mapping in the ionosphere at the equatorial plane, *Planet. Space Sci.*, *18*(2), 259–263, doi:10.1016/0032-0633(70)90161-3.

Ott, E. (1978), Theory of Rayleigh-Taylor bubbles in the equatorial ionosphere, *J. Geophys. Res.*, *83*(A5), 2066–2070, doi:10.1029/JA083iA05p02066.

Perkins, F. (1973), Spread *F* and ionospheric currents, *J. Geophys. Res.*, *78*(1), 218–226, doi:10.1029/JA078i001p00218.

Pfaff, R., et al. (2010), Observations of DC electric fields in the low-latitude ionosphere and their variations with local time, longitude, and plasma density during extreme solar minimum, *J. Geophys. Res.*, *115*, A12324, doi:10.1029/2010JA016023.

Retterer, J. M. (2005), Physics-based forecasts of equatorial radio scintillation for the Communication and Navigation Outage Forecasting System (C/NOFS), *Space Weather*, *3*, S12C03, doi:10.1029/2005SW000146.

Retterer, J. M. (2010), Forecasting low latitude radio scintillation with 3-D ionospheric plume models: 1. Plume model, *J. Geophys. Res.*, *115*, A03306, doi:10.1029/2008JA013839.

Roddy, P. A., D. E. Hunton, J. O. Ballenthin, and K. M. Groves (2010), Correlation of in situ measurements of plasma irregularities with

ground-based scintillation observations, *J. Geophys. Res.*, *115*, A06303, doi:10.1029/2010JA015288.

Scherliess, L., and B. G. Fejer (1999), Radar and satellite global equatorial *F* region vertical drift model, *J. Geophys. Res.*, *104*, 6829–6842, doi:10.1029/1999JA900025.

Valladares, C. E., R. Sheehan, and J. Villalobos (2004), A latitudinal network of GPS receivers dedicated to studies of equatorial spread *F*, *Radio Sci.*, *39*, RS1S23, doi:10.1029/2002RS002853.

J. O. Ballenthin, P. A. Roddy, and Y.-J. Su, Space Vehicles Directorate, Air Force Research Laboratory, Kirtland AFB, NM 87117, USA.

E. Dao and M. C. Kelley, School of Electrical and Computer Engineering, Cornell University, Ithaca, NY 14853, USA. (mck13@cornell.edu)

D. L. Hysell, Department of Earth and Atmospheric Sciences, Cornell University, Ithaca, NY 14853, USA.

R. F. Pfaff, Laboratory for Extraterrestrial Physics, NASA Goddard Space Flight Center, Greenbelt, MD 20771, USA.

J. M. Retterer, Institute for Scientific Research, Boston College, Chestnut Hill, MA 02467, USA.